Short communication

In-situ observation of inhomogeneous degradation in large format Li-ion cells by neutron diffraction

Lu Cai [a], Ke An [a,*], Zhili Feng [b], Chengdu Liang [c], Stephen J. Harris [d]

[a] *Chemical and Engineering Materials Division, Oak Ridge National Laboratory, Oak Ridge, TN 37831, USA*
[b] *Materials Science and Technology Division, Oak Ridge National Laboratory, Oak Ridge, TN 37831, USA*
[c] *Center for Nanophase Materials Sciences, Oak Ridge National Laboratory, Oak Ridge, TN 37831, USA*
[d] *Lawrence Berkeley National Laboratory, Berkeley, CA 94720, USA*

HIGHLIGHTS

► *In-situ* probe degradation mechanisms in large format cells by neutron diffraction.
► The fresh cell has a spatially uniform (homogeneous) local state of charge.
► The degraded cell shows a spatially inhomogeneous deterioration.
► Capacity losses in the cathode and anode are coupled.
► Remediation strategies should focus on location-specific issues in the cell.

ARTICLE INFO

ABSTRACT

This work presents a non-destructive *in-situ* method for probing degradation mechanisms in large format, operating, commercial lithium-ion batteries by neutron diffraction. A fresh battery (15 Ah capacity) was shown to have a uniform (homogeneous) local state of charge (SOC) at 4.0 V (9 Ah SOC) and 4.2 V (15 Ah SOC), with 1.33 C and 2.67 C charging rates, respectively. This battery was then aggressively cycled until it retained only a 9 Ah capacity, 60% of its original value. Inhomogeneous deterioration in the battery was observed: near the edges, both the graphite anode and the spinel-based cathode showed a significant loss of capacity, while near the central area, both electrodes functioned properly. An SOC mapping measurement of the degraded battery in the fully charged state (4.2 V) indicated that the loss of local capacity of the anode and cathode is coupled.

1. Introduction

Service life is one of the main challenges in applications of lithium-ion batteries to the automobile market [1]. Many studies have investigated the capacity loss/degradation at the material level, promoting our understanding of degradation mechanisms [2,3]. For layered $LiMO_2$ (M = Co, Ni, Al, or/and Mn) cathodes, degradation is mainly due to: 1. loss of electronic contact resistance [4]; 2. inhomogeneous local state-of-charge (SOC) [5,6]; and 3. NiO-like phases near the surface and grain boundaries [7]. $LiMn_2O_4$-based spinel cathode studies have shown that the dissolution of manganese leads to the degradation of active materials [1,8–12]. Premanand et al. [9] studied a commercial Li-ion battery (1.05 Ah) with a $LiMn_2O_4$-based spinel cathode and a carbon anode. After the battery degraded, they cut it open and confirmed the formation of λ-MnO_2 on the cathode and the deposition of MnO on the anode from XRD. Lee et al. [13] reported that repeated lattice contraction/expansion during cycling causes the breakdown of the spinel structure.

As Li-ion batteries are complicated electrochemical systems, the study of their degradation mechanisms requires sophisticated tools. At the material level, disassembly of batteries is usually required to detect the problems microscopically or locally. However, cell level studies using non-destructive and *in-situ* diagnostics are especially important, since cutting the batteries open may change the chemistry and will prevent repeated measurements on

* Corresponding author.
  E-mail address: kean@ornl.gov (K. An).

the same system. Neutron diffraction is one such technique, and the neutron's high penetration power enables the simultaneous observation of both cathode and anode [14]. For example, Senyshyn et al. [15] captured cathode and anode information on fresh and fatigued cylindrical Li cells.

This study probes the degradation mechanisms of a large format commercial Li-ion battery cell (dimension of 200 × 120 × 5 mm) designed for electric vehicles. Commercial Li-ions batteries are chosen for this study because their standardized and high quality manufacturing processes minimize cell production errors. Larger cells are especially likely to have inhomogeneities, which have been suggested to be the ultimate cause of cell degradation [16]. In this study we relate the presence of inhomogeneities to degradation for large format Li-ion batteries.

2. Experimental

The investigated commercial battery has the original capacity of 15 Ah with graphite anode and spinel $Li_xMn_2O_4$-based cathode. The battery was charged/discharged at 40 °C in an isothermal chamber. The neutron diffraction measurements were conducted using the VULCAN instrument, an engineering diffractometer at the Spall-ation Neutron Source (SNS), Oak Ridge National Laboratory (ORNL) [17,18]. The collected d-spacing ranges from 0.5 Å to 2.5 Å. The measured spot volume was confined as 10 (vertical) × 5 (horizontal) × 5 (along the beam) mm^3 using the incident beam slit and collimators. Neutron diffraction data were collected either at the charged states (4.0 V or 4.2 V) or during charging/discharging cycles before and after degradation. For mapping at the charged states, the collection time at each location was about 1.5 h for each pattern. As for charging/discharging, neutron data were collected continuously, and then sliced by the VDRIVE software [19] based on the statistics of the diffraction pattern. Each pattern corresponds to 15 min collection time.

3. Results and discussion

3.1. The fresh cell has a spatially uniform (homogeneous) local SOC

The investigated commercial fresh battery was charged to 60% of its total capacity (∼9 Ah at 4.0 V) using a 20 A charging current. After a more than 1 h battery rest, neutron diffraction data were collected at 9 locations (see the "X" in Fig. 1a). The measured lattice parameters of the spinel cathode at all 9 spots, which are related to

the state of charge SOC (the amount of Li$^+$ in the crystal structure [20]), are identical within the fitting errors (∼8.137 Å) (Fig. 1b). The anode contains LiC_6 (stage 1 lithium-intercalated graphite com-pound), LiC_{12} (stage 2), and residual graphite; no other interme-diate stages present. The LiC_6 (002), LiC_{12} (004), and graphite (004) peaks can be identified in Fig. 2a. The molar fractions of these anode phases, an indication of the amount of Li$^+$ intercalated in the graphite anode, can be calculated by the intensity ratio of these (00*l*) peaks ($I_{(00l)} \propto M \times |F_{(00l)}|^2/V^2$, where M is the molar fraction, $F_{(00l)}$ is the structure factor for scattering from the plane (00*l*), V is the unit cell volume). The peak intensities ($I_{(00l)}$) are calculated by the single peak fitting in GSAS using time-of-flight profile function 3 [21,22]. The molar fractions of LiC_6, LiC_{12}, and graphite are around 10%, 85%, and 5% with minor scatter. The battery was later charged from 2.7 V to 4.2 V using a higher current of 40 A (2.67 C charging rate) until its total capacity (∼15 Ah) was reached, and the data were collected without any battery resting. Point 1 has 56(±3)% LiC_6, 35(±3)% LiC_{12}, and 9(±2)% graphite, while the molar ratio of LiC_6:LiC_{12}:graphite was almost the same as at Point 5 (55(±2):37(±3):8(±1)). The lattice parameter of the cathode is 8.056(±0.002) Å at the two spots. Therefore, the fresh battery demonstrates homogeneous local SOC, even after the fast charging.

3.2. The degraded cell shows a spatially inhomogeneous deterioration

The cell was continuously cycled at 40/−40 A charging/dis-charging currents in an isothermal chamber at 40 °C for more than 400 cycles. It retained about 9 Ah capacity, which is about 60% of its original value. Whereas Points 1 and 5 have identical local states of charge for the fresh cell charged to 60% and 100% of its total ca-pacity, in the degraded cell significant inhomogeneity in the local SOC was found. In this case, Point 5 lost little of any capacity, while Point 1 showed strong signs of deterioration. Fig. 2 shows a com-parison of neutron diffraction patterns in the non-degraded and degraded cases at 9 Ah SOC. Comparing with the non-degraded condition (Fig. 2a and b), the anode at Point 1 shows weaker LiC_{12} (004), LiC_{12} (112), LiC_6 (002), and Li_xC_6 ($x = 0.5$ or 1) (110) peaks but stronger graphite (004) peaks than that at Point 5 in the degraded condition (Fig. 2c and d). The lower intensities of Li_xC_6 ($x = 0.5$ or 1) peaks prove the loss of the ability to intercalate lithium ions for the anode at Point 1. Meanwhile, the intensity of the cathode (222) decreases with the appearance of a new peak at higher d-spacing at Point 1. To get better idea how these two Points
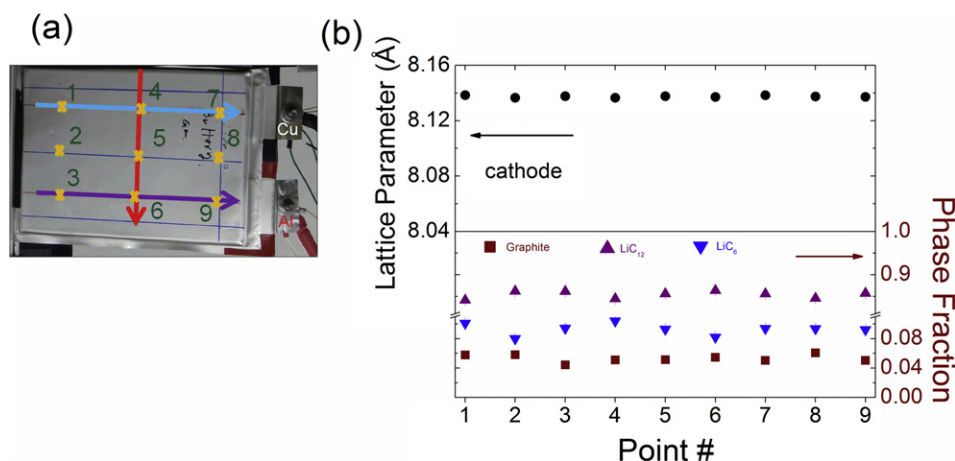

Fig. 1. (a) Photo of the commercial battery. "X" and arrows show the scanning locations and directions. (b) At 4.0 V (SOC ∼9 Ah), the lattice parameter of the cathode and the molar fraction of graphite, LiC_{12}, and LiC_6 at 9 spots indicated by the cross symbols in (a).
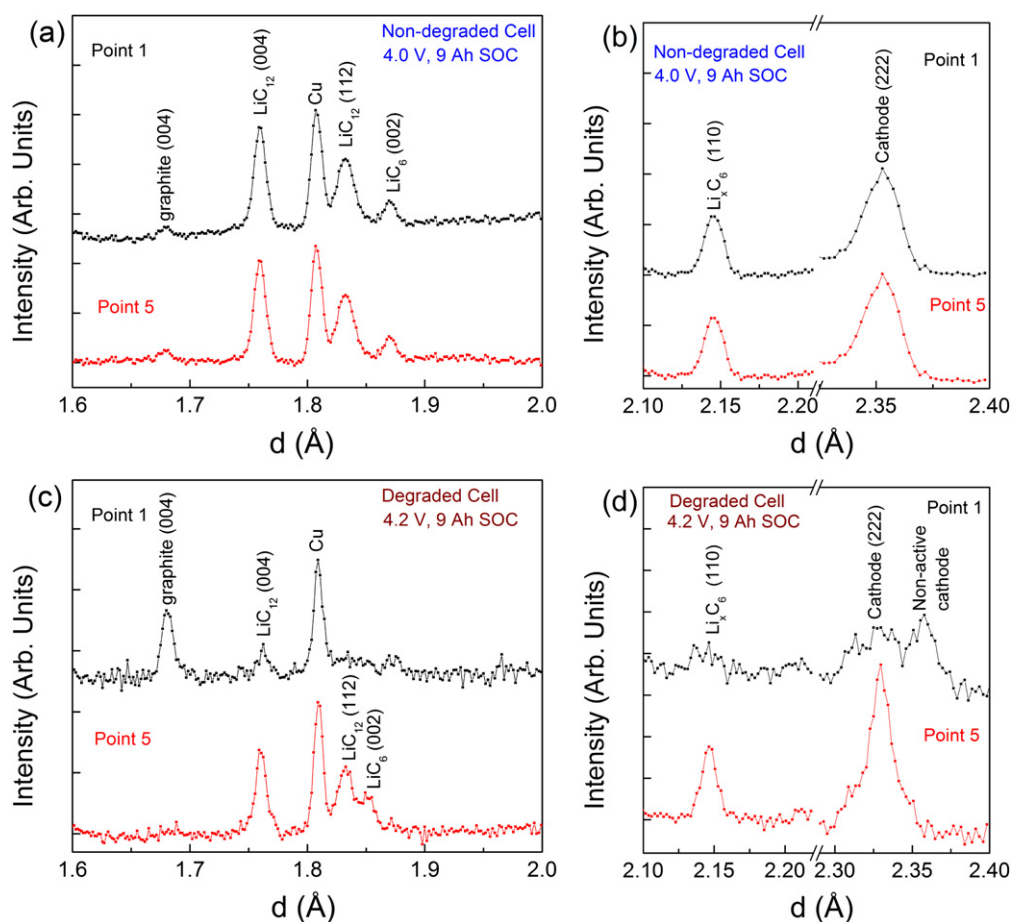
Fig. 2. Neutron diffraction patterns in selected areas between 1.6 and 2.1 Å (a) (b) non-degraded cell, (c) (d) degraded cell.

function differently, neutron diffraction data were collected during cycling (the charging/discharging currents are 2/−2 A), as shown in Fig. 3. At Point 5 (Fig. 3a), the d-spacing of (222) of the cathode decreases during charging, as Li ions intercalate into the graphite layer to form LiC_{12} and then LiC_6. During discharging, the d-spacing of (222) follows the reverse path to its uncharged state. At the same time, LiC_6 transitions to LiC_{12} and then to graphite. Transport of Li^+ between the cathode and anode is revealed by the gradual d-spacing variations of the cathode and the corresponding structural evolution in the anode. In Fig. 3b, at Point 1, unlithiated graphite remains the major phase throughout the cycle, indicating that few Li ions intercalate into the anode. As for the spinel cathode, the (222) peak splits into two peaks at an early stage of charging. The d-spacing of the less intense peak evolves normally (the same with Point 5), but the more intense peak exhibits only small changes, showing a limited Li^+ insertion/removal process. This peak may be identified with the first two strong diffraction peaks (131) and (004) of Li_2MnO_3 [23,24], which can be formed during the spinel decomposition [8]. However, the formation of Li_2MnO_3 cannot be confirmed because the remaining diffraction peaks of Li_2MnO_3 overlap with those from other phases.

The structural evolution of the spinel cathode at Point 5 during cycling (the charging/discharging currents are 2/−2 A) before and after degradation is shown in Fig. 4. In the degraded condition, the lattice parameter of cathode varies much faster than in the non-degraded case. However, the total volume contraction during charging (or the total volume expansion during discharging) at Point 5 is the same for both conditions, indicating that the same

amount of Li^+ is extracted or inserted locally. At the fully charged state (4.2 V), the lattice parameters are 8.056(2) Å and 8.061(2) Å before and after degradation, respectively. At the fully discharged state (2.7 V), the lattice parameters are identical within the fitting error (8.201(4) Å for non-degraded and 8.195(2) Å for degraded). The reason for the faster variation of lattice parameter at the degraded state is that Point 5 has to be charged to a higher local SOC than the average SOC due to the deteriorated areas like Point 1. Thus, the presence of inhomogeneous capacity leads to greater local SOC values, which can itself cause additional degradation.

3.3. Capacity losses in the cathode and anode are coupled

More than 40 locations in the degraded cell were probed after being charged to 4.2 V. The arrows in Fig. 1a show the lines scanned. Fig. 5a shows neutron diffraction patterns along the upper horizontal lines (where points 1, 4, and 7 are located). The points at horizontal locations of 10 mm, 20 mm, 30 mm, 170 mm, and 180 mm show a considerable amount of unlithiated graphite but limited amounts of LiC_{12} and LiC_6. These areas also show less intense of cathode (222) peak with evolving of a new peak (this peak demonstrates limited changes in Fig. 3b and thus limited Li^+ insertion/removal abilities during electrochemical cycling), proving a large amount of uncharged cathode material. Thus, degradation on charging occurs in both the cathode and the anode.

This coupled phenomenon is analyzed quantitatively by calculating the uncharged graphite phase fraction and comparing to the
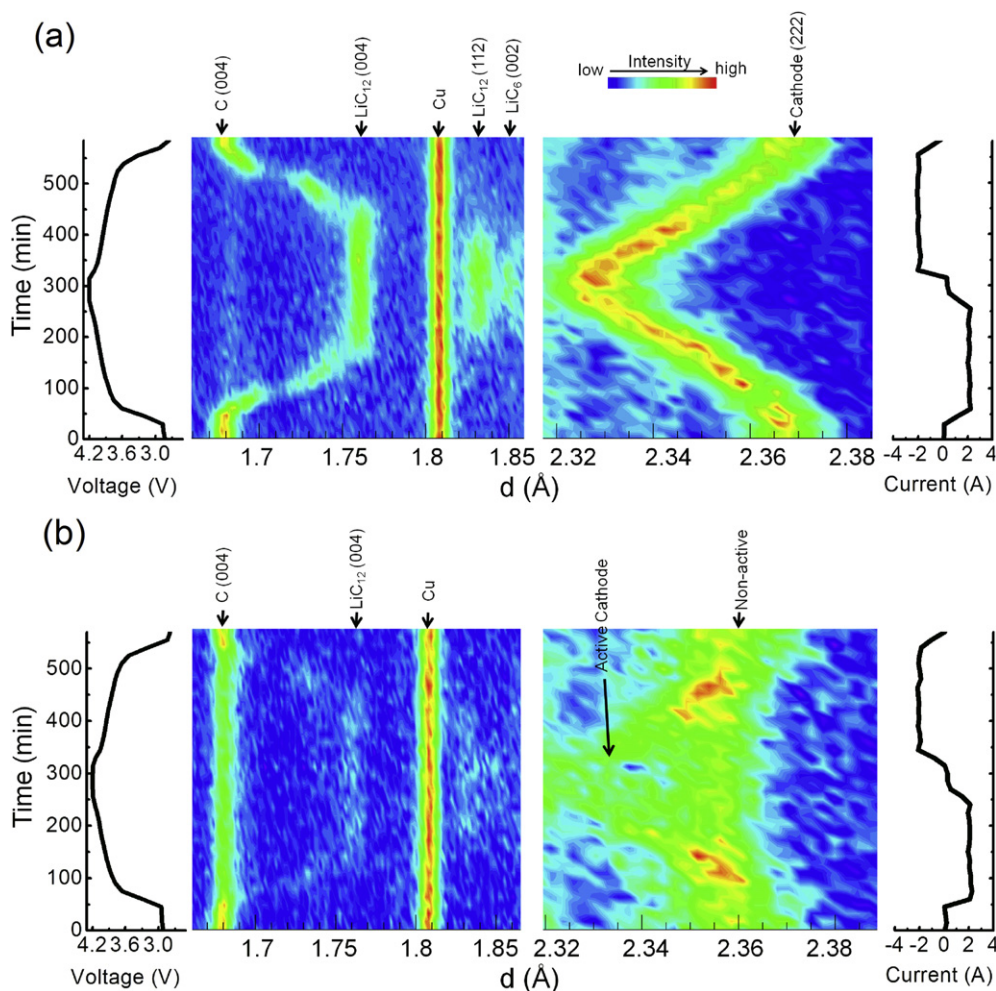
Fig. 3. (a) Left vertical axis, time vs. voltage. Right vertical axis, current for the degraded cell. (Middle) contour plot of 32 neutron diffraction patterns during cycling at Point 5. (b) At Point 1.

normalized intensity of (222) peak of the active cathode material. The Cu current collector is taken as the internal standard. The normalized intensity of (222) peak is calculated by the intensity of (222) from the single peak fitting by GSAS [21,22] divided by the intensity of Cu (111) peak. In Fig. 5b, along both horizontal lines, the uncharged graphite phase mole fraction is close to 80% near the left edge at 10 mm. It decreases to less than 20% between 100 and 160 mm and then increases to 40% at ∼180 mm along the upper horizontal line. Meanwhile, the amount of active cathode material

Fig. 4. A comparison of lattice parameter evolution of the cathode between 2.7 V and 4.2 V for both fresh and degraded cells at Point 5.

is minimal close to 10 mm in both horizontal lines, as shown in Fig. 5b, and it increases toward 100 mm. After ∼160 mm, the amount of active cathode material decreases again along the upper line. The same finding also occurs along the vertical line in Fig. 1a. Thus, degradation at the anode and at the cathode occurs in the same locations.

There may be many factors contributing to the capacity losses, for example, electrolyte solution loss (dry out), separator pore clogging, non-uniform temperature distribution during operation, and loss of active materials [2,3,8–10,25,26]. Neutron diffraction can only detect the changes in crystalline electrodes and in current study the coupled loss of functionality in both the cathode and the anode may be due to loss of active materials or the breakdown of Li$^+$ diffusion pathways. The Mn^{2+} in the active spinel cathode dissolves into the electrolyte after many cycles [8–11]. Mn^{2+} or MnO is then deposited on the carbon anode [8,9], which may block the Li$^+$ diffusion path (higher impedance), resulting in a corresponding loss of graphite function. Another possible reason for the coupling is that unwanted gas is generated from the spinel dissolution/decomposition or electrolyte decomposition. This degassing may then lead to damage of the corresponding electrodes materials connections as well as to their contacts to the current collectors. Accumulation of gasses has been inferred from the swelling of the battery pouch in the fully discharged state.
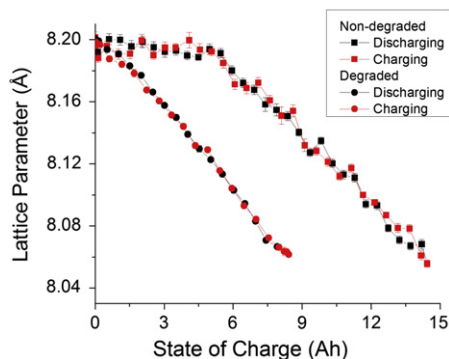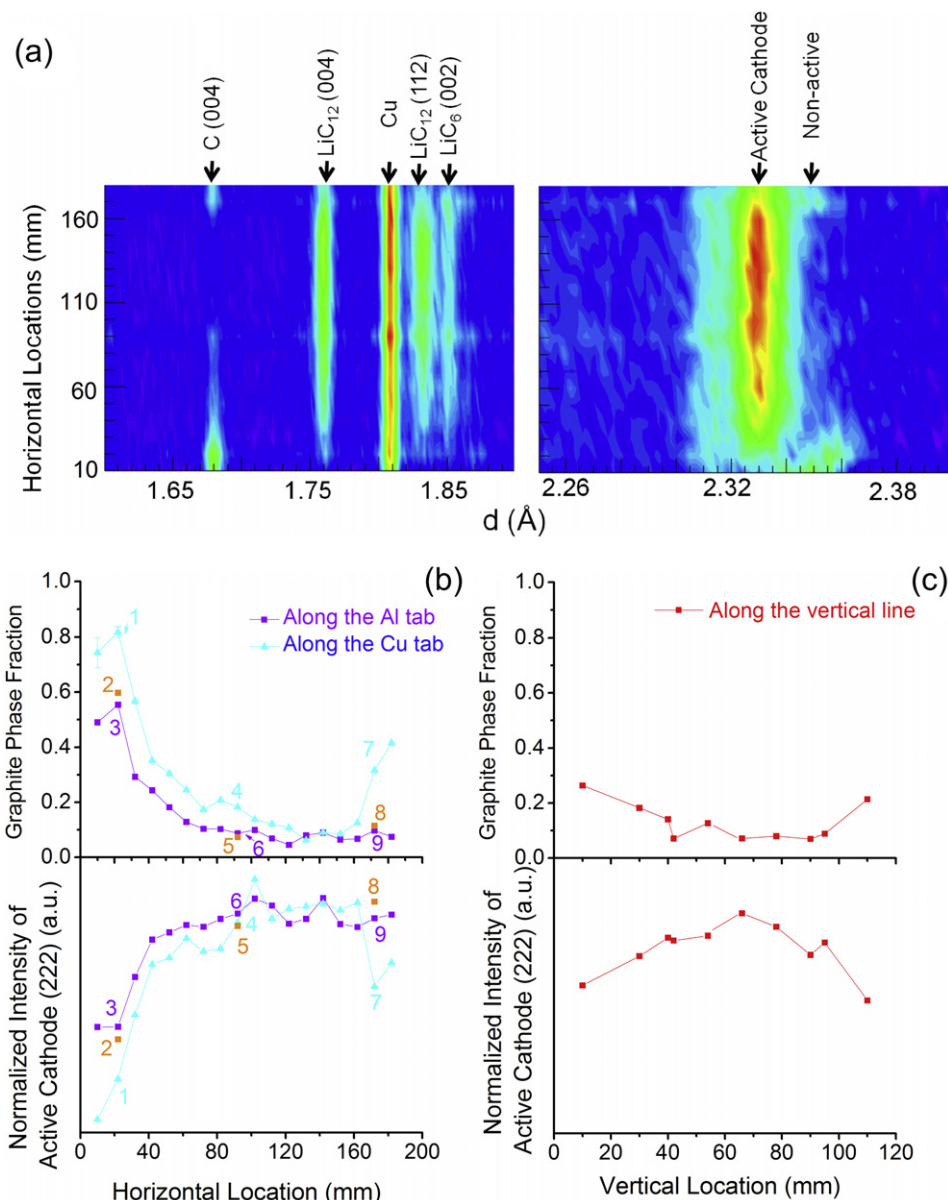
Fig. 5. At 4.2 V, (a) contour plots of neutron diffraction patterns along the blue line in Fig. 1(a) (the Cu tab). (b) Graphite mole fraction and the normalized intensity of cathode (222) along the blue line (the Cu tab) and the purple line (the Al tab) and (c) along the red line (the vertical line). Location number is labeled in (b). (For interpretation of the references to color in this figure legend, the reader is referred to the web version of this article.)

4. Conclusion

Our results show that degradation cannot in general be considered to be a homogeneous process in commercial pouch cells. While the non-degraded cell has the homogeneous local SOC, the degraded cell exhibits spatially heterogeneous deterioration. When the cell lost 40% of its original capacity, part of the cell functioned normally (tends to be near the center), while part degraded severely (close to the edge). The degradation (capacity loss) is coupled in both the cathode and anode, which may be contributed from the coupled loss of active materials. Remediation steps will be different compared to a cell that degraded uniformly by 40%.

Acknowledgment

References

[1] J.B. Goodenough, Y. Kim, Chem. Mater. 22 (2010) 587–603.
[2] P. Arora, R.E. White, M. Doyle, J. Electrochem. Soc. 145 (1998) 3647–3667.
[3] L.S. Kanevskii, V.S. Dubasova, Russ. J. Electrochem. 41 (2005) 1–16.
[4] M. Kerlau, M. Marcinek, V. Srinivasan, R.M. Kostecki, Electrochim. Acta 53 (2007) 1385–1392.
[5] J. Nanda, J. Remillard, A. O'Neill, D. Bernardi, T. Ro, K.E. Nietering, J.Y. Go, T.J. Miller, Adv. Funct. Mater. 21 (2011) 3282–3290.
[6] J.L. Lei, F. McLarnon, R. Kostecki, J. Phys. Chem. B 109 (2005) 952–957.
[7] Y. Kojima, S. Muto, K. Tatsumi, H. Kondo, H. Oka, K. Horibuchi, Y. Ukyo, J. Power Sources 196 (2011) 7721–7727.
[8] J. Christensen, J. Newman, J. Electrochem. Soc. 152 (2005) A818–A829.
[9] R. Premanand, A. Durairajan, B. Haran, R. White, B. Popov, J. Electrochem. Soc. 149 (2002) A54–A60.

[10] J. Vetter, P. Novak, M.R. Wagner, C. Veit, K.C. Moller, J.O. Besenhard, M. Winter, M. Wohlfahrt-Mehrens, C. Vogler, A. Hammouche, J. Power Sources 147 (2005) 269—281.
[11] Y.Y. Xia, Y.H. Zhou, M. Yoshio, J. Electrochem. Soc. 144 (1997) 2593—2600.
[12] J.C. Hunter, J. Solid State Chem. 39 (1981) 142—147.
[13] J.H. Lee, J.K. Hong, D.H. Jang, Y.K. Sun, S.M. Oh, J. Power Sources 89 (2000) 7—14.
[14] X.L. Wang, K. An, L. Cai, Z. Feng, S.E. Nagler, C. Daniel, K. Rhodes, A.D. Stoica, H.D. Skorpenske, C. Liang, W. Zhang, J. Kim, Y. Qi, S.J. Harris, Sci. Rep. 2 (2012) 747.
[15] A. Senyshyn, M.J. Muhlbauer, K. Nikolowski, T. Pirling, H. Ehrenberg, J. Power Sources 203 (2012) 126—129.
[16] D. Kehrwald, P.R. Shearing, N.P. Brandon, P.K. Sinha, S.J. Harris, J. Electrochem. Soc. 158 (2011) A1393—A1399.
[17] K. An, H.D. Skorpenske, A.D. Stoica, D. Ma, X.L. Wang, E. Cakmak, Metall. Mater. Trans. A 42A (2011) 95—99.
[18] X.L. Wang, T.M. Holden, A.D. Stoica, K. An, H.D. Skorpenske, A.B. Jones, G.Q. Rennich, E.B. Iverson, Mater. Sci. Forum 652 (2010) 105—110.
[19] K. An, VDRIVE — Data Reduction and Interactive Visualization Software for Event Mode Neutron Diffraction, ORNL Report, Oak Ridge National Laboratory, ORNL-TM-2012-621, 2012.
[20] H. Berg, H. Rundlov, J.O. Thomas, Solid State Ion. 144 (2001) 65—69.
[21] B.H. Toby, J. Appl. Crystallogr. 34 (2001) 210—213.
[22] R.B. Von Dreele, A.C. Larson, Los Alamos National Laboratory Report, LAUR 86-748, 1994.
[23] A. Boulineau, L. Croguennec, C. Delmas, F. Weill, Chem. Mater. 21 (2009) 4216—4222.
[24] P. Strobel, B. Lambertandron, J. Solid State Chem. 75 (1988) 90—98.
[25] U.S. Kim, C.B. Shin, C.S. Kim, J. Power Sources 180 (2008) 909—916.
[26] Y.Y. Xia, M. Yoshio, J. Electrochem. Soc. 143 (1996) 825—833.